

# A data assimilation approach to discharge estimation from space

Jeffrey Neal,<sup>1\*</sup>  
Guy Schumann,<sup>1</sup>  
Paul Bates,<sup>1</sup>  
Wouter Buytaert,<sup>1</sup>  
Patrick Matgen<sup>2</sup>  
and Florian Pappenberger<sup>3</sup>

<sup>1</sup> School of Geographical Sciences,  
University of Bristol, Bristol BS8 1SS,  
UK

<sup>2</sup> Public Research Centre—Gabriel  
Lippmann, Belvaux L-4422,  
Luxembourg

<sup>3</sup> European Centre for Medium-Range  
Weather Forecasts, Reading RG29AX,  
UK

\*Correspondence to:

Jeffrey Neal, School of Geographical  
Sciences, University of Bristol, Bristol  
BS8 1SS, UK.

E-mail: j.neal@bristol.ac.uk

## Abstract

River discharge is currently monitored by a diminishing network of gauges, which provide a spatially incomplete picture of global discharges. This study assimilated water level information derived from a fused satellite Synthetic Aperture Radar (SAR) image and digital terrain model (DTM) with simulations from a coupled hydrological and hydrodynamic model to estimate discharge in an un-gauged basin scenario. Assimilating water level measurements led to a 79% reduction in ensemble discharge uncertainty over the coupled hydrological hydrodynamic model alone. Measurement bias was evident, but the method still provided a means of improving estimates of discharge for high flows. The study demonstrates the potential of currently available synthetic aperture radar imagery to reduce discharge uncertainty in un-gauged basins when combined with model simulations in a data assimilation framework, where sufficient topographic data are available. The work is timely because in the near future the launch of satellite radar missions will lead to a significant increase in the volume of data available for space-borne discharge estimation. Copyright © 2009 John Wiley & Sons, Ltd.

**Key Words** data assimilation; discharge estimation; hydraulic model; SAR

## Introduction

Remote sensing from space-borne platforms offers a potentially cost-effective method of monitoring components of the hydrological cycle, including river discharge, at global scales (Biggin and Blyth, 1996). Unfortunately, discharge cannot be measured directly from these platforms with current technology and so the use of observable hydraulic variables such as water level, width, sinuosity and area as proxies to estimate discharge has been suggested (see reviews by Smith, 1997; Alsdorf and Lettenmaier, 2003; Brakenridge *et al.*, 2005; Alsdorf *et al.*, 2007). Images collected by Synthetic Aperture Radar (SAR) sensors have proven particularly useful for flood monitoring due to their all weather capabilities, and ability to penetrate vegetation cover at some wavelengths (Alsdorf *et al.*, 2007). For example, Bjerklie *et al.* (2003) developed river discharge estimation equations using multiple-regression, based on over 1000 independent discharge measurements, whilst Smith and Pavelsky (2008) used the correlation between effective widths upstream and ground-based measurements of discharge to forecast discharge up to 8 days ahead with a mean absolute error of <25%. These techniques indicate that there are usable signals in remotely sensed SAR data, but exploiting these requires direct measurements of discharge at some point in the catchment.

An alternative way of using observed data is to combine it with a dynamic model to obtain an optimal estimate of a geophysical field of interest. This process, known as data assimilation, has been widely applied to remotely sensed data for atmospheric and hydrological applications (Walker *et al.*, 2003; Reichle, 2008). An advantage of this approach is that it considers both model simulations and the image-derived measurement data when estimating state variables such as level and discharge, without the need for ground observations. Furthermore, if integrated with parameter-estimation techniques (Vrugt *et al.*, 2005), there is the potential to estimate uncertain model parameters, which may be used to increase the accuracy of the simulation model. This is particularly relevant in un-gauged basins where

Received 27 May 2009  
Accepted 9 October 2009

often very few data are available to drive hydrological simulation models of discharge.

Data assimilation techniques based on versions of the Kalman filter have been used to assimilate ground-gauge-based river level data at points along river reaches (Madsen and Skotner, 2005; Neal *et al.*, 2007) from which one method of estimating discharge is to use state augmentation (Madsen and Cañizares, 1999). However, the need to use ground-based river level data is a major limitation for globally applicable techniques. Applications of assimilation techniques with remotely sensed water level data are rare. In one of the few studies of this type, Andreadis *et al.* (2007) successfully used a square root Ensemble Kalman Filter (EnKF) (Evensen, 2004) to assimilate synthetic water level measurements from a proposed swath altimetry satellite (Alsdorf *et al.*, 2007) with simulations from the LISFLOOD-FP two-dimensional hydraulic model (Bates and De Roo, 2000). However, an assimilation study of this type has yet to be attempted using real observations in an un-gauged basin scenario. Accordingly, in this paper, shoreline heights derived from SAR imagery and a Light Detection and Ranging (LiDAR)-based digital terrain model (DTM) were assimilated with model simulations from a coupled hydrological and hydrodynamic model to explore the potential for reducing errors in discharge and water level estimates in un-gauged basins with space-borne SAR imagery. The reasons why the SAR data and proposed method do not represent a gauge replacement strategy are also discussed in the Section on Results.

## Methods and Data

A 10-km reach of the River Alzette (Luxembourg) with a history of flooding and an average floodplain width of

around 300 m was selected for this study. The experimental setup used 76 channel cross sections and a 2-m resolution DTM derived from LiDAR (Figure 1b), with ~15 cm vertical accuracy, as a definition of topography for a one-dimensional hydrodynamic model. This hydrodynamic model was driven by simulations of discharge at its upstream boundary taken from a simple hydrological model that uses European Centre for Medium-Range Weather Forecasts ERA interim climatological data for precipitation estimates. For this site, a 25-m resolution C-band Envisat Advanced Synthetic Aperture Radar (ASAR) image taken ~4 h after peak discharge of a one in 5-year recurrence interval flood event, which occurred on 2 January 2003 (Figure 1a), was acquired for assimilation with hydrodynamic model simulations. Further event data were available in the form of field water levels taken during the event and gauge data above the upstream boundary (Figure 1d). Both of these were reported previously by Matgen *et al.* (2007) and are retained for model evaluation. For the extraction of water heights, flood shorelines derived from the SAR image were intersected with the LiDAR-derived DTM (Figure 1c) to estimate water levels along the reach for assimilation. The setup of each of these components is described in the following.

### Data assimilation

Sequential data assimilation methods can be used to assimilate time-dependent model state forecasts with measurements as they become available. For linear dynamics, the Kalman filter provides an optimal sequential assimilation method, in that it minimizes state variance based on both model forecast and measurement error covariance. For nonlinear dynamics, the extended Kalman filter can be used for forward integration of the

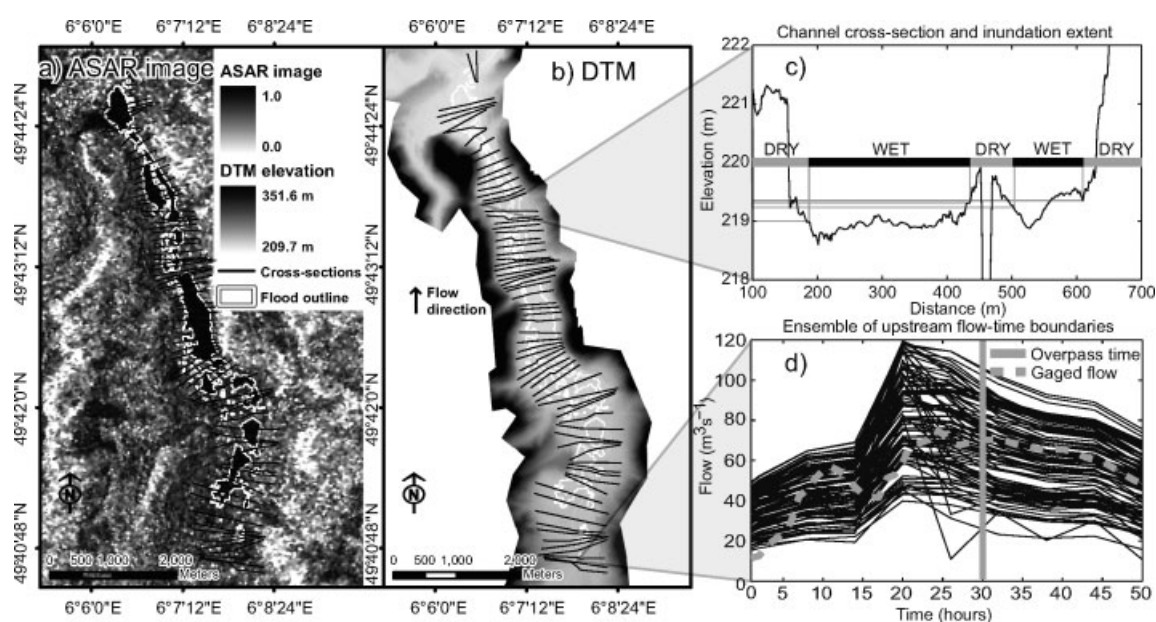


Figure 1. Diagram showing (a) ASAR image of 2003 flood event on the River Alzette with flood outline and river cross-section locations; (b) DTM and cross-section locations; (c) illustration of water level extraction method from inundation extent and cross sections and (d) ensemble of upstream boundary conditions from a simple hydrological model

error covariance, but becomes very expensive computationally as the problem dimensionality increases (Reichle, 2008). An alternative solution is to approximate error covariance using an EnKF, where errors are defined by the difference between each ensemble member and the ensemble mean (Evensen, 2003). The EnKF was adopted here because it provides a framework for considering uncertainty in both model simulations and measurement data, and has been applied successfully to nonlinear models and ensembles where the state variables of interest are not normally distributed (as is the case here). The filter was also used to update simulated flows by augmenting them with the water levels in the state vector (Madsen and Cañizares, 1999).

### Hydrological modelling

The Alzette river basin was treated as un-gauged, and, therefore, only data that have not been measured *in situ* were used by the hydrological model. In this study, we used predictions of convective and stratiform precipitation and evaporation from the ERA interim reanalysis dataset (Simmons, 2006). Daily forecasts issued at 12 p.m. with lead times of 3, 6, 9 and 12 h were converted into time series with a temporal resolution of 6 h. The ERA interim data do not close the water balance, whilst the evaporation data are known to contain large errors (For the study region, they were nearly as high as the precipitation data, suggesting an overestimation). Therefore, a correction factor was added to the evaporation data in order to allow the hydrological model control over the water balance of the catchment. Assuming a lack of any information regarding the internal hydrological processes of the catchment, a widely used simple conceptual model was implemented. The catchment moisture deficit store of Croke and Jakeman (2004) was used as a loss module, whilst routing was implemented as a linear store (Beven, 2001). This results in a model with two parameters, controlling respectively the catchment water balance and response velocity, as well as two state variables that need to be initialized. The parameters are summarized in Table I. However, a longer-than-necessary warming-up period from the start of the ERA interim data set in 1990 was used to minimize the impact of model state initialization. Errors in reanalysis data are likely to be quite large, thus it should be noted that the parameterization of the hydrological model that might result from any parameter-estimation scheme is expected to be effective. This is an inherent problem with the use of these data, although they are more skilful than climatology, which in turn means that they are better than guessing.

The model was run in a Monte Carlo simulation with parameter sets that were drawn from a prior uniform range of feasible parameter values (Table I) to generate 100 ensemble members. As the parameter ranges can be very wide, particularly for conceptual models, further constraining was done by selecting only model results that gave peak discharges during the study period within the range of 30–100 m<sup>3</sup> s<sup>-1</sup>. These limits were

Table I. Hydrological model parameters and ranges sampled

	Minimum	Maximum
Loss module		
Initial soil moisture deficit (m)	0	1.5
Flow threshold (m)	0.1	2
Ratio between stress and flow thresholds	0	1
Routing module		
Initial flow (m/h)	0	0.05
Linear reservoir time constant (h)	1	10

This table includes initialisation parameters that are not important given the long warm-up period.

determined by expert judgment, similar to the limits of acceptability approach of Beven (2006).

### Hydrodynamic model

A one-dimensional hydrodynamic model of the reach based on the Hydrologic Engineering Centers River Analysis System (HEC-RAS) code was used, with the floodplain conveyance accounted for by extending the cross sections onto the floodplain based on the LiDAR DEM (Pappenberger *et al.*, 2006; Schumann *et al.*, 2007a). The cross sections were a composite of ground survey data in the channel and floodplain terrain heights extracted from the LiDAR DTM. The model required a hydrograph as its upstream boundary condition (Figure 1d), which in this case was derived from the hydrological model simulations described above, and specification of the friction (Manning's *n*) at each cross section. Estimates of global channel roughness of 0.035 and global floodplain roughness of 0.05 were made on the basis of the physical characteristics of a river of this type (Acrement and Schneider, 1984).

The use of channel cross-section data limits the applicability of the methodology as such data are often unavailable in un-gauged basins to a reasonable level of accuracy and may have to be estimated (e.g. using geomorphic relationships). The model is expected to be sensitive to the treatment of channel bathymetry, meaning the use of less accurate bathymetric data is likely to affect simulation accuracy. To crudely simulate this scenario, the cross-section data were simplified to a trapezoidal channel using the channel-restricted cross-section point filtering tool in HEC-RAS, creating a second 'simple bathymetry' hydrodynamic model. An alternative approach would be to estimate channel bathymetry as part of the data assimilation methodology (Durand *et al.*, 2008).

### SAR data processing

Flood extent was estimated by classifying the ASAR image into dry and wet pixels using a simple radiometric threshold technique (Deshmukh and Shinde, 2005). To account for uncertainty in the image threshold value, this was repeated four times using threshold values equally spaced between digital numbers 120 and 150. These

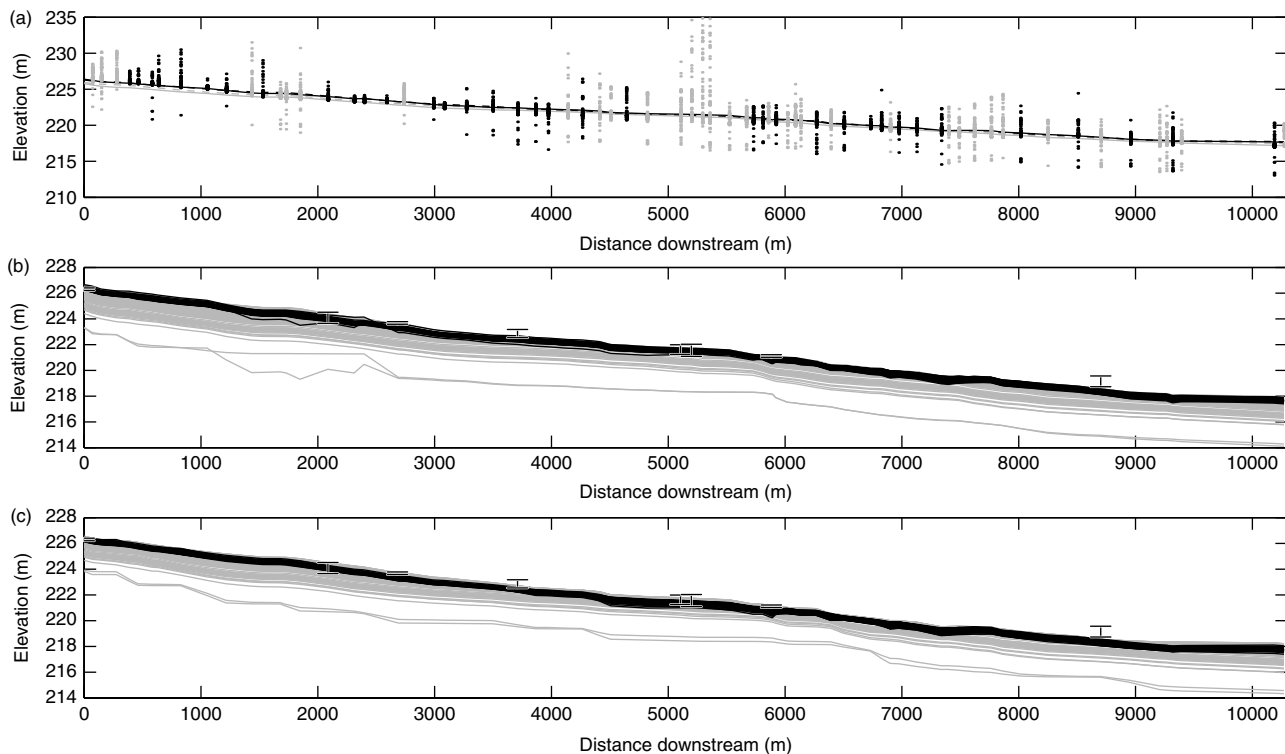


Figure 2. (a) Plot of measurement ensembles derived from the ASAR image, which were retained for assimilation (dark dots) and rejected (light dots). Level simulations at the time of the satellite overpass before and after assimilation are also shown. (b) Plot of ensemble levels before (lighter lines) and after (darker line) assimilation along with water levels measured in the field. (c) Plot of ensemble water levels before and after assimilation along with water levels measured in the field using the simple channel geometry

were chosen to represent the range of threshold values expected for this image given specular reflectance over open water. The ASAR image was geo-located using four ground control points easily locatable on bridges and road crossings, then fine tuned using the Monte Carlo-based image shifting technique described in Schumann *et al.* (2008). A comparison with independent check points suggests that this resulted in a standard deviation of geo-location errors of 19.4 m, which was found to be the largest source of uncertainty in water stage estimates from this image by Schumann *et al.* (2008).

The EnKF required an ensemble of measurements to represent measurement uncertainty. To achieve this, the four flood edge estimates derived from the image classification were repeatedly shifted in space according to the estimated geo-location error above. These new shoreline locations were then intersected with the DTM, as illustrated by Figure 1c and described in more detail by Schumann *et al.* (2008), to yield the ensemble of water level estimates shown in Figure 2a. Measurement error covariance was defined from the perturbations of this ensemble around the mean. Thus, if  $\mathbf{Y}$  is a matrix of  $N$  ensemble perturbations from the ensemble mean, then the measurement error covariance matrix  $\mathbf{R}_e$  is defined as follows (Evensen, 2003):

$$\mathbf{R}_e = \frac{\mathbf{Y}\mathbf{Y}^T}{N - 1} \quad (1)$$

In Figure 2a, the cluster of high points at ~5000 m downstream was caused by a steep road embankment bordering

the flood edge. These measurements are clearly incorrect and introduce bias into the mean of the measurements. This was not unexpected as it is often noted that the combination of remotely sensed imagery of this resolution and a near-valley filling event (like the one observed here) tends to be more sensitive to over-prediction of water levels than on-site measurements. This is because the ground elevation rapidly increases at the valley side relative to the floodplain as a whole, whilst any vegetation heights not removed from the raw LiDAR data tend to increase the elevation of the DTM. However, the spatial coverage offered by the remote sensing means it is not necessary to use all measurements derived from the image. Here only half the measurements were assimilated (darker dots in Figure 2a) by considering only those with the smallest inter-quartile range over the ensemble at a particular location, thus favouring measurement locations with relatively flat topography and small classification uncertainty. The size of this subsample came about by removing samples until no measurement mean increased by more than twice the expected LiDAR error (0.15 m) in the downstream direction. The idea here was to remove measurements that are hydraulically incoherent due to steep topography or image classification errors. Ranking samples based on topographic slope or a normality test and removing half the locations resulted in a broadly similar subset of measurements. The sub-sampling method does not completely remove measurement bias but reduces its impact as the retained measurement ensembles show less evidence of skew towards higher elevations. Although the

subsample of measurements is used for most of the experiments here, the effect of assimilating different numbers of measurements locations is assessed in the Section on Sensitivity to Geometry and Number of Measurements. More advanced processing techniques based on active contouring methods that fuse with the DTM (Mason *et al.*, 2007) could be used to improve upon the water level estimates and further reduce the bias, although this latter technique is not easily applicable at this site due to fragmentation of the flooded area (Figure 1a).

### Evaluation data

Maximum water level data were available from a survey of wrack marks at five locations and three automatic stage readings at bridges (Matgen *et al.*, 2007) where localized surcharging may have increased water levels. The wrack mark measurements represent peak water level around 4 h before the satellite overpass but are subject to uncertainty due to geo-location errors (as they were collected with a handheld global positioning system (GPS)) and errors in the DTM off which the heights were sampled. Levels at these measurement locations were compared with the level at the closest hydrodynamic model cross section. A flow gauge 7 km above the upstream end of the site was also retained for evaluating posterior flow estimates. To evaluate the model flow estimates, the gauge discharge was assumed to represent reach average discharge as there are no major tributaries along the reach. However, the errors introduced by converting gauged levels to flow via a rating curve were significant relative to other model uncertainties, especially at high flows. Pappenberger *et al.* (2006) found the uncertainty range in this gauge to be at least  $\pm 11\text{--}16\text{ m}^3\text{ s}^{-1}$  when assessing the influence of rating curve uncertainty on flow estimates. Therefore, the evaluation conducted here is limited by these gauge errors and a lack of repeat independent data for this or other events, a problem common to many flood inundation studies (Bates, 2004).

## Results and Discussion

The hydrodynamic model, built from the surveyed cross-section geometry, was used to simulate water levels using the ensemble of 100 hydrographs in Figure 1d generated by the hydrological model. From these the water levels at the time of the satellite overpass were extracted. Each simulation took under 1.9 s on an Intel 2.99 GHz core 2 processor such that this is a practical approach for real-time applications. Figure 2b shows simulated levels for each cross section in the model as light lines, with the mean shown as the bold light line in Figure 2a. Over the length of the reach, the average of the inter-quartile ranges and standard deviation of simulated levels at each cross section was 0.66 and 0.65 m respectively. The darker lines in Figure 2b plot simulated water levels after assimilating the SAR-derived measurements, which are shown as dark dots in Figure 2a. Again, the ensemble mean is shown as a

same shade bold line. The reach average inter-quartile range and standard deviation of these post-assimilation estimates was 0.12 and 0.09 m respectively. Therefore, assimilating the SAR-derived water level data led to a significant reduction in water level uncertainty over that derived from the hydrological model flow ensemble alone, as would be expected from an EnKF given the measurement and forecast variance. The filter maintained the shape of the water surface at most locations, with reductions in water surface slope around 1500 and 5000 m retained in the post-assimilation water level estimates. This would not have been the case if a linear regression of the measurement data had been used to estimate water levels as in Schumann *et al.* (2007b). Physically unrealistic water surfaces after assimilating the measurements are evident in two of the ensemble members around 2000 m downstream, whilst negative or flat water surface slopes were estimated around 7500 m, indicating how the assimilation process itself is not error free. The root mean squared error between the ensemble mean and field stages fell from 0.7 to 0.4 m, whilst mean error fell from 0.7 to 0.3 m. Uncertainty in each field stage was estimated by Schumann *et al.* (2007a), resulting in ranges of  $\pm 0.10$  to  $\pm 0.47$  m for each measurement, as shown by the error bars in Figure 2b. Given these uncertainties and the time lag between peak flow and the satellite overpass, the post-assimilation water level estimates are a credible estimate of the true water levels given the available field data.

The results in Figure 2 demonstrate that assimilating the SAR-derived water levels reduced the average water level standard deviation from 0.65 to 0.09 m; however, the value of this reduction in comparison to assimilating ground data is not yet clear. One way to assess this, for an idealized situation, is to assimilate synthetic ground measurements with pre-defined error statistics instead of the SAR measurements and compare the results. To do this, a single simulation was run using the gauged flows and optimal roughness parameters of 0.042 obtained by Schumann *et al.* (2007a) when calibrating the hydrodynamic model to the field stages used in this study. From this simulation, levels were extracted at the overpass time, then corrupted with pre-defined uncorrelated random noise and assimilated in place of the SAR-derived measurements. The average water level standard deviation after assimilating measurements at one to three locations with error standard deviations between 0.05 and 0.16 m are plotted in Figure 3a. Over the 10-km domain, two ground measurements with standard deviations below 0.04 m were able to provide similar reductions in water level uncertainty to the SAR-derived measurements. To give this context, gauging stations in Europe are usually constructed every 10–60 km. Thus, even over the 10-km reach length used here, the SAR image provides spatially distributed high flow level data that would only be available from a relatively dense and accurate network of ground measurements.

The expected errors in ground measurements vary for many reasons, especially if based on water marks, but it

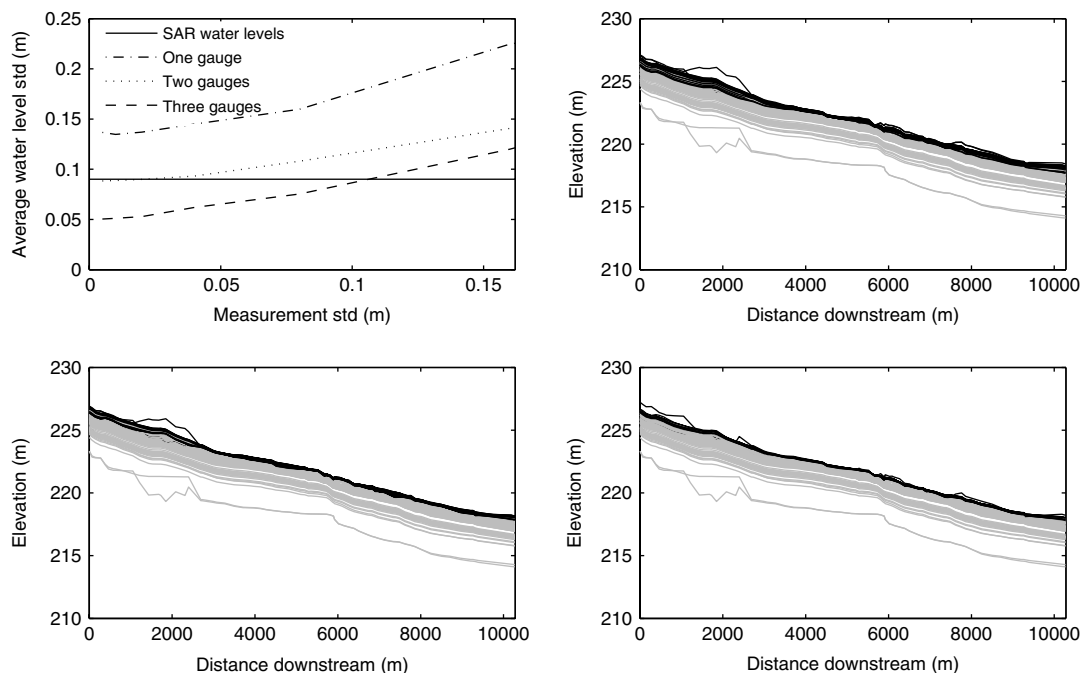


Figure 3. (a) Plot of average water level against measurements standard deviations. Plots of ensemble water levels before (light lines) and after (dark lines) assimilation of 1 (b), 2 (c) and 3 (d) measurements with standard deviation of 0.04 m

is not unreasonable to expect measurements at gauging stations to be accurate to a few centimetres. Given this expectation, Figure 3b–c plots the prior and posterior level ensembles given 1, 2 and 3 ground measurements with a standard deviation of 0.04 m. By assimilating one ground measurement, the posterior ensemble at the measurement location was more constrained than was possible with the SAR data, but less so over the whole domain because the ensemble error covariance between the measurement location and other model cross sections decreased with distance. This decrease is likely to be greater if the hydrodynamic model were considered as a source of uncertainty in the experimental design. However, a gauging station would probably also operate at low flow and provide a much greater temporal resolution, which would propagate downstream over time to increase the spatial influence of the gauge. Therefore, it should be stressed that a gauge would provide level data, especially in the time dimension, that are not attainable from currently available SAR imagery. For this reason, the use of SAR imagery in a data assimilation framework should not be viewed as an alternative to ground gauges.

### Estimating flow

Estimates of prior and posterior flows are shown in Figure 4, along with the gauged flows of  $75.0 \text{ m}^3 \text{ s}^{-1}$  and the 5th and 95th percentile of the uncertainty range ( $\pm 0.16 \text{ m}^3 \text{ s}^{-1}$ ) from Pappenberger *et al.* (2006). The filter reduced the flow standard deviation by 79% from  $21.1$  to  $4.4 \text{ m}^3 \text{ s}^{-1}$ . Prior to assimilation, the ensemble mean flow of  $60.5 \text{ m}^3 \text{ s}^{-1}$  was  $14.5 \text{ m}^3 \text{ s}^{-1}$  lower than the gauge estimate, whilst after assimilation the ensemble mean flow of  $85.1 \text{ m}^3 \text{ s}^{-1}$  was  $10.1 \text{ m}^3 \text{ s}^{-1}$  greater than the gauge estimate. Given that errors in gauged

ratings when extrapolated for high flows are up to 20% for this gauge (Pappenberger *et al.*, 2006), this is a credible but possibly an overly high estimate of the flow. This overestimation could be partly due to uncertainty in the hydrodynamic model parameters or the rating applied to the gauge data. However, it is indicative of an inherent weakness in using water level estimates derived from imagery of near-valley filling events, in that they are skewed towards over-prediction due to the valley shape, and become more so with coarser image resolutions. Thus, direct measurements of water level (such as, for large rivers, those from the proposed satellite swath altimetry mission surface water ocean topography (SWOT) (<http://swot.jpl.nasa.gov/>)) should offer a fundamental improvement over those derived here because they are digital elevation model (DEM) independent. However, supplementing direct altimetry measurements with measurements derived from imagery would reduce the time lag between measurements during high flows.

This study has neglected sources of uncertainty from the hydrodynamic modelling as these were assumed to be small relative to uncertainty in the SAR-derived water levels and hydrological modelling. However, the hydrodynamic model is known to be a source of error in that the parameter, process and topographic representation are uncertain. These will become more significant if the hydrological model parameters are more accurately defined (Pappenberger *et al.*, 2007). Thus, future work will need to address the magnitude of hydrodynamic model uncertainty in relation to other errors associated with the hydrological model, measurement data and assimilation process, as well as the topographic detail required to capture the first-order flow hydraulics.

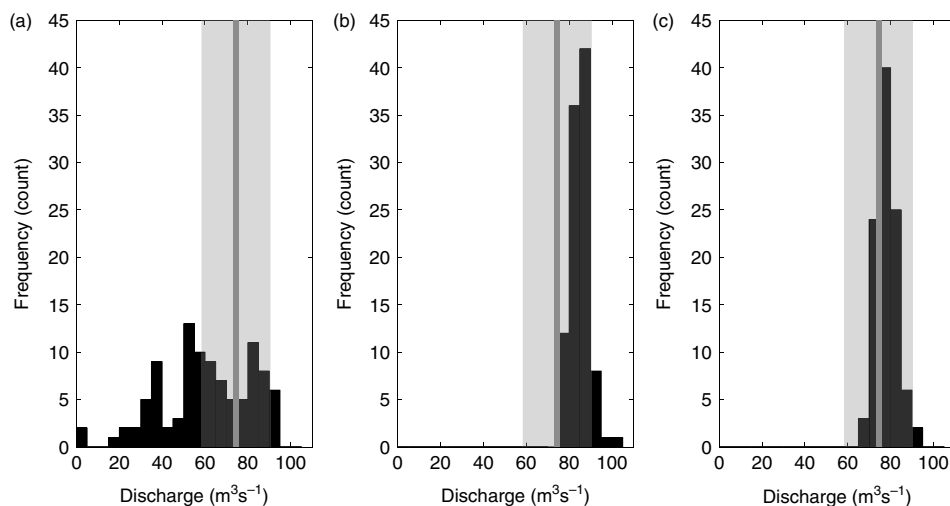


Figure 4. Histograms of estimated flow before (a) and after assimilating measurement data using the full cross section (b) and simple geometry (c) channel models. Gauged flow and its uncertainty are also shown

The low temporal frequency of current imagery is a significant problem on a river of this size. Image sequences through the same flood event that capture peak flow are unlikely, whilst a flood may be missed altogether. Nevertheless, ongoing satellites launches in the COSMO-SkyMed constellation and upcoming missions such as those in the European Space Agencies Global Monitoring for Environment and Security (GMES) initiative will increase the temporal density of flood extent imagery. There is currently no consensus on which river reaches this technique will be appropriate for, whilst topographic data of the quality used here are not universally available. A lack of sufficient topographic data is currently a significant barrier to the widespread implementation of the method (Sanders, 2007), although the availability of DEM data is steadily improving and the channel bathymetry could be sampled infrequently relative to water levels, or even possibly estimated as part of the assimilation process (Durand *et al.*, 2008). The method needs to be tested with lower resolution and less accurate topographic information if the range of sites where it can be applied is to increase. Furthermore, larger rivers and those with tributaries may require larger ensembles to represent error covariance or filters that only update states that are spatially close to the measurements.

#### *Sensitivity to geometry and number of measurements*

This section assesses the sensitivity of the data assimilation scheme to two key changes in the model setup, namely, using the simplified channel geometry and adjusting the number of SAR measurements assimilated. These changes are assessed independently such that the experimental setup is identical to that above except for a change in geometry or the number of measurements.

A key problem with using detailed cross-section geometry is that it is unlikely to be available in many un-gauged basins. Trapezoidal or rectangular channels

require less data to parameterize and have been used successfully by numerous studies (Trigg *et al.*, 2009), but often exhibit reduced accuracy over models with more detailed geometry. Despite this loss of detail, it may still be possible to obtain more accurate estimates of discharge than from the hydrological model alone. Figure 2c plots the prior level simulations as light lines and the posterior level estimate as dark lines using the simplified channel geometry introduced in the Section on Hydrodynamic Model. The simple geometry reduced channel conveyance leading to higher levels for a given flow, which increased the ensemble mean by an average of 0.20 m, indicating that the model is sensitive to the treatment of geometry. The posterior water levels were more alike, with the ensemble means differing by an average of 0.02 m along the reach due to the dominance of the SAR-derived measurements over the prior simulations. As the channel conveyance has declined, the posterior best estimate of discharge (Figure 4c) has decreased relative to the full geometry model (Figure 4b) by  $7.1 \text{ m}^3 \text{ s}^{-1}$  to  $78.0 \text{ m}^3 \text{ s}^{-1}$ , which by chance is closer to the gauge estimate of  $75.0 \text{ m}^3 \text{ s}^{-1}$  than the full geometry model. This suggests that there is potential for using the method with quite simple channel data, although this cannot be confirmed with a single study site.

During the processing of the SAR-derived levels, many locations were rejected under the assumption that where topography is steep or image classification is uncertain the level measurement may be biased towards higher elevations. This assumption was tested by assimilating measurements from between 10 and 70 locations, which have been ranked by their inter-quartile range (smallest to greatest). Some results of this experiment are shown in Figure 5, with the prior water level simulations and ensemble mean plotted in Figure 5a. Figure 5b plots the reach average flow ensemble and its mean after assimilating measurements from 10–70 locations. As expected, the discharge uncertainty decreases as more measurements are assimilated; however, the ensemble mean also increases (away from the gauged flow of  $75.0 \text{ m}^3 \text{ s}^{-1}$ ) as

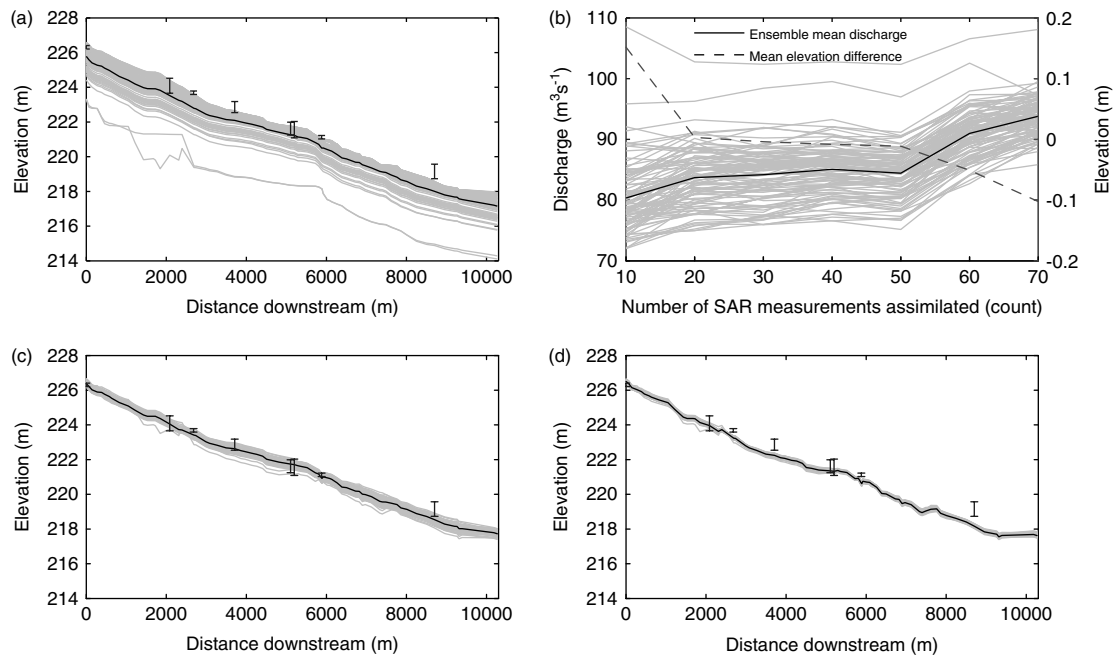


Figure 5. (a) prior level simulations from Figure 2b. (b) Posterior flow estimates after assimilating 10–70 SAR-derived measurements and mean difference in level estimates from Figure 2b. (c) Plot of ensemble water levels before and after assimilation 10 SAR measurements. (d) Plot of ensemble water levels before and after assimilation 70 SAR measurements

the measurement bias is introduced from 60 measurement locations and upwards. Discharge estimates are relatively similar for between 20 and 50 measurement locations as is the mean difference in water level from the results from the Section on Results and Discussion. Therefore, it is essential that the SAR-derived levels are subject to some form of quality control prior to assimilation and that the image is not assumed to provide suitable data everywhere. Figure 5c and d plots the posterior level ensembles after assimilating measurements from 10 and 70 locations, respectively. Obviously assimilating 70 measurement locations led to less spread in the ensemble than assimilation of 10 measurement locations. However, the 70 measurement locations plot indicates a further reason for not assimilating all SAR locations, in that the posterior water level profile has diverged from a hydraulically plausible surface as it contains many locations where the level increases with distance downstream. Thus, as many locations are unsuitable for extracting water heights, it is essential to consider measurement error before using this type of data.

## Conclusions

The test case has shown that where detailed digital elevation data are available it is possible to retrieve discharge and level estimates from 25-m resolution ASAR imagery when combined with hydrodynamic modelling using a data assimilation approach. These estimates were consistent with independent water level and discharge evaluation data, although there is evidence of bias towards higher water levels in the SAR-derived data. Notably, in an un-gauged basin scenario, the SAR-derived measurements led to a significant reduction in discharge uncertainty and error. This uniquely demonstrates the

application of an EnKF for river discharge estimation with currently available SAR imagery and hydrodynamic model simulations in an un-gauged basin scenario. The discharge estimates could be used to constrain the hydrological model parameters, which may improve forecasts or predictions made by the hydrological model when measurement data are unavailable. The method therefore has the potential to improve discharge predictions in un-gauged basins and provide reliable information on extreme high flows not easily observable over large scales from the ground. However, it is essential that the SAR-derived levels are subject to some form of quality control prior to assimilation and that the image is not assumed to provide suitable data everywhere.

The SAR-derived data are not a substitute for a dense *in situ* gauge network, as they are only applicable infrequently at high flow and are likely to be less accurate than *in situ* gauge data at local scales. A significant drawback of the method demonstrated here is the need for good topographic data both within channel and on the floodplain, whilst expert judgement was used to establish the prior discharge estimate. Such problems can be minimized as channel geometry can be collected infrequently relative to water level measurements. Moreover, the use of a simplified trapezoidal channel at this site still improved the posterior discharge estimate over the hydrological model alone. Nevertheless, further tests of the method with less accurate and lower-resolution topographic data are required.

## Acknowledgements

Jeffrey Neal was funded by the Flood Risk Management Research Consortium (FRMRC), supported by grant number EP/F20511/1 from the EPSRC. Guy Schumann

was funded by a Great Western Research fellowship. Patrick Matgen was funded by the Hydrasens project, financed by the National Research Fund of the Grand Duchy of Luxembourg and the Belgian Science Policy. The authors would like to thank the reviewers for their valuable contribution to the development of this paper.

## References

- Acrement GJ, Schneider VR. 1984. *Guide for Selecting Manning's Roughness Coefficients for Natural Channels and flood plains*. Report No. FHWA-TS-84-204. Federal Highways Administration, US Department of Transportation: Washington, D.C., 62 pp.
- Alsdorf DE, Rodriguez E, Lettenmaier DP. 2007. Measuring surface water from space. *Reviews of Geophysics* **45**: DOI:10.1029/2006RG000197.
- Alsdorf DE, Lettenmaier DP. 2003. Tracking fresh water from space. *Science* **301**(5639): 1491–1494.
- Andreadis KM, Clark EA, Lettenmaier DP, Alsdorf DE. 2007. Prospects for river discharge and depth estimation through assimilation of swath-altimetry into a raster-based hydrodynamics model. *Geophysical Research Letters* **34**: DOI:10.1029/2007GL02972.
- Bates PD. 2004. Remote sensing and flood inundation modelling. *Hydrological Processes* **18**: 2593–2597.
- Bates PD, De Roo APJ. 2000. A simple raster-based model for flood inundation simulation. *Journal of Hydrology* **236**(1–2): 54–77.
- Beven KJ. 2001. *Rainfall-Runoff Modelling. The Primer*. John Wiley and sons: Chichester; 360 pp.
- Beven K. 2006. A manifesto for the equifinality thesis. *Journal of Hydrology* **320**: 18–36.
- Biggin DS, Blyth K. 1996. A comparison of ERS-1 satellite radar and aerial photography for river flood mapping. *Journal of the Institution of Water and Environmental Management* **10**: 59–64.
- Bjerklie DM, et al. 2003. Evaluating the potential for measuring river discharge from space. *Journal of Hydrology* **278**(1–4): 17–38.
- Brakenridge GR, Nghiem SV, Anderson E, Chien S. 2005. Space-Based Measurement of River Runoff, *Eos Transactions*. AGU, **86**(19): 185, DOI:10.1029/2005EO190001.
- Croke B, Jakeman A. 2004. A catchment moisture deficit module for the ihacres rainfall-runoff model. *Environmental Modelling and Software* **19**: 1–5.
- Deshmukh KS, Shinde GN. 2005. An adaptive color image segmentation. *Electronic Letters on Computer Vision and Image Analysis* **5**(4): 12–23.
- Durand MD, et al. 2008. Estimation of bathymetric depth and slope from data assimilation of swath altimetry into a hydrodynamic model. *Geophysical Research Letters* **35**: L20401. DOI:10.1029/2008GL034150.
- Evensen G. 2003. The Ensemble Kalman Filter: theoretical formulation and practical implementation. *Ocean Dynamics* **53**: 343–367.
- Evensen G. 2004. Sampling strategies and square root analysis schemes for the EnKF. *Ocean Dynamics* **54**(6): 539–560.
- Madsen H, Cañizares R. 1999. Comparison of extended and ensemble Kalman filters for data assimilation in coastal area modeling. *International Journal for Numerical Methods in Fluids* **31**(6): 961–981.
- Madsen H, Skotner C. 2005. Adaptive state updating in real-time river flow forecasting—a combined filtering and error forecasting procedure. *Journal of Hydrology* **308**(1–4): 302–312.
- Mason DC, et al. 2007. Use of fused airborne scanning laser altimetry and digital map data for urban flood modelling. *Hydrological Processes* **21**(11): 1436–1447.
- Matgen P, et al. 2007. Integration of SAR-derived river inundation areas, high-precision topographic data and a river flow model toward near real-time flood management. *International Journal of Applied Earth Observation and Geoinformation* **9**(3): 247–263.
- Neal JC, et al. 2007. Flood inundation model updating using an ensemble Kalman filter and spatially distributed measurements. *Journal of Hydrology* **336**(3–4): 401–415.
- Pappenberger F, et al. 2006. Influence of uncertain boundary conditions and model structure on flood inundation predictions. *Advances in Water Resources* **29**(10): 1430–1449.
- Pappenberger F, et al. 2007. Grasping the unavoidable subjectivity in calibration of flood inundation models: a vulnerability weighted approach. *Journal of Hydrology* **333**(2–4): 275–287.
- Reichle R. 2008. Data assimilation methods in the Earth sciences. *Advances in Water Resources* **31**: 1411–1418. DOI:10.1016/j.advwatres.2008.01.001.
- Sanders B. 2007. Evaluation of on-line DEMs for flood inundation modeling. *Advances in Water Resources* **30**: 1831–1843.
- Schumann G, et al. 2007a. Deriving distributed roughness values from satellite radar data for flood inundation modelling. *Journal of Hydrology* **344**: 96–111.
- Schumann G, et al. 2007b. High-resolution 3D flood information from radar imagery for flood hazard management. *Transactions on Geoscience and Remote Sensing* **45**(6): 1715–1725.
- Schumann G, et al. 2008. Conditioning water stages from satellite imagery on uncertain data points. *IEEE Geoscience and Remote Sensing Letters* **5**(4): 810–813.
- Simmons A, et al. 2006. ERA-Interim: new ECMWF reanalysis products from 1989 onwards. *ECMWF Newsletter* **110**: 25–35.
- Smith LC. 1997. Satellite remote sensing of river inundation area, stage, and discharge: a review. *Hydrological Processes* **11**(10): 1427–1439.
- Smith LC, Pavelsky TM. 2008. Estimation of river discharge, propagation speed, and hydraulic geometry from space: Lena River, Siberia. *Water Resources Research* **44**(3): W03427, DOI:10.1029/2007WR006133.
- Trigg M, et al. 2009. Amazon flood wave hydraulics. *Journal of Hydrology* **374**(1–2): 92–105. DOI:10.1016/j.jhydrol.2009.06.004.
- Vrugt JA, et al. 2005. Improved treatment of uncertainty in hydrologic modeling: combining the strengths of global optimization and data assimilation. *Water Resources Research* **41**: W01017.
- Walker JP, et al. 2003. New remote sensing technologies require advances in hydrologic data assimilation. *EOS, American Geophys Union* **84**(49): 545–551.